Nationaal Lucht- en Ruimtevaartlaboratorium
National Aerospace Laboratory NLR

NLR-TP-98265

Outline and application of GEROS: a European grid generator for rotorcraft simulation methods

M.H.L. Hounjet

C.B. Allen

L. Vigevano, N. Trivellato

A. Pagano, A. D'Alascio, N. Jobard

Nationaal Lucht- en Ruimtevaartlaboratorium
National Aerospace Laboratory NLR

NLR-TP-98265

Outline and application of GEROS: a European grid generator for rotorcraft simulation methods

M.H.L. Hounjet

C.B. Allen*

L. Vigevano**, N. Trivellato**

A. Pagano***, A. D'Alascio***, N. Jobard***

* *University of Bristol*
** *Politecnico di Milano (PMI)*
*** *Centro Italiano Ricerche Aerospaziali S.C.p.A. (CIRA)*

This investigation has been carried out under a contract awarded by the European Commission, contract number BRPR-CT96-0162, and partly as a part of NLR's basic research programme, Working Plan number A.1.C.2.

This report is based on a presentation to be held on the ECCOMAS 98 Conference, 7-11 September 1998, Athens, Greece.

Division:	Fluid Dynamics
Issued:	June 1998
Classification of title:	unclassified

Summary

GEROS is the name of a grid generator system for the modelling of complex multi-bladed rotors under development in Europe as a part of the development of a complete rotorcraft simulation method: The Brite/EuRam
EROS project. The grid generator [7] exploits a CHIMERA domain decomposition on structured grids. The development is being carried out by rotorcraft manufacturers
(Agusta, ECD, GKN-Westland), research centres (CIRA, DERA, DLR, NLR, ONERA), and Universities (Polit. Milano, Univ. Bristol, Univ. Glasgow, Univ. Rome 3).

This paper discusses the capabilities of the GEROS grid generator and presents relevant results.

Contents

1 Introduction

The efficient application/development of computer methods to determine the unsteady flow about realistic rotorcraft configurations poses specific requirements (multiple bodies in relative motion; dynamic, deforming and periodic grids; far field resolution) to the grids and the grid generating procedures. The EROS consortium has developed a CHIMERA [3] type grid generator for application to advanced rotorcraft blades for the modelling of single and multiblade simulations in hover and in forward flight aiming at solving the aforementioned problems.[1]

The CHIMERA approach is selected for its natural adaptation to flow and dynamic geometry characteristics (complexities), reduced wall clock times by simplifying grid generation, better accuracy using shape conforming grids and short familiarization times. The approach has been applied to rotorcraft already by many researchers [10, 12, 15, 5, 1]. The often repeated drawbacks of the CHIMERA approach, namely that defects in conservation of flow fluxes might lead to impaired solutions, is considered to be of minor importance as other sources of uncertainty coming from the geometrical state description of the structure (hinge angles, mass and stiffness) are larger. Add to this also that the quality of the grids has a similar impact [11]. Also the setting up of the connectivity (which is approximately $O(N^{\frac{2}{3}}, N$ is number of cells) is supposed to be a smaller task compared with generating the connectivity involved in unstructured methods. The latter need dynamic adaptation to resolve flow gradients properly and have to upgrade the connectivity for a major part of the flow domain ($O(N)$). Further, since the geometric modelling is hard to decouple, the grid generator addresses the full spectrum of the dynamic geometrical problem: surface grid generation, volume grid generation, volume grid adaptation/ deformation/ rotation/ positioning, dynamic connectivity and animation/ prototyping of the dynamic geometries.

At present the basic components of the method have been realized and research is being directed at improving the critical components in the process cycle. The paper presents the past development and status of the GEROS gridgenerator and shows relevant results.

[1] Extension to complete rotorcraft is straightforward

2 General features of GEROS code

This chapter summarizes the features of the GEROS method. GEROS exploits the CHIMERA domain decomposition on structured grids and approaches an all-in-one capability for grid generation by providing the following key features:

- Surface grid generation
- Volume grid generation
- Volume grid dynamics (deformation and motion)
- Volume grid a posteriori quality enhancement
- Volume grid quality analysis
- Volume grid elliptic smoothing
- Volume grid CHIMERA tagger (connectivity arranger)
- Coded in FORTRAN77 with FORTRAN90 extensions
- Interactive control with on-line help functionality
- Visual inspection and prototyping
- Script driven batch operations
- Script control.

The embedded script facility allows the gridding process to be repeatable and to be documented. It is also helpful when adaptation is required for the surface grids in which case a new surface grid can be generated based on the original input data by a reversed call of the solver. The prototyping feature allows the inspection and animation of the location and other characteristics of the deforming grids and their connectivity in relative motion for all azimuthal angles and blades prior to the CFD simulation.

The main structure of the GEROS code which is divided into 6 subsystems to perform the aforementioned main tasks is depicted in figure 1. The main actions that can be requested by a user are controlled by the **GEROS main menu** which allows the user to indicate a required action, to abort the program legally or to continue to a lower level menu. Thereafter the control menu associated with the requested action will appear, in which the user is allowed to edit the process control parameters and to perform the requested action. Next the user has the option to visualize the results of the action and to save the state of the action. After a surface grid generation/ volume grid generation/ upgrading/ simulation (deforming-positioning)/ tagging/ visualization with GEROS the program returns to the main menu. The modelling applied in the submodules is explained in the next chapter.

2.1 GEROS process

Applying the GEROS system for the simulation of the geometry of a rotor requires initially:

- an aerodynamic jig-shape geometry of the blades and
- a jig-shape elastomechanical model

The basic operations necessary for a simulation session are in chronological order:

- **Geometry manipulation** on aerodynamic geometry parts (main blade, tip).
- **Surface grid generation** on aerodynamic geometry parts.
- **Volume Grid generation** initiated from the surface grids.
- **Volume Grid generation** of background grid.
- **Volume Grid generation** of intermediate Cartesian grids.
- **Volume Grid generation** of tip-vortex grids.
- **CHIMERA tagging** of the whole setup.
- **Simulation** of the geometry and connectivity for a realistic motion/deformation.

2.2 Input and output

The main bulky input of the grid generator consist of:

- Sets of parent surface grids forming a network for which a single-block surface grid is generated.
- Surface grids for which a single-block volume-grid is generated.
- The control angles of the hinges and the elastic deformation.
- Volume grids to which upgrading/ simulation (deforming-positioning)/ tagging/ visualization might be applied.

The bulky output of the generator consist of: surface grids; volume grids and connectivity tables.

2.3 Visualization

The VISUAL3 [6] library is used to plot depending on the type of generation:

- 3-D views of selected grid planes.
- 3-D views of selected grid planes or mesh cuts coloured according to the quality indicators.
- 3-D views of the hole locations, the fringe locations and the support points.

The aforementioned plots might be static or dynamic (i.e. versus azimuthal angle).

3 Modelling

This chapter describes the characteristics of models and features embedded in the GEROS code.

3.1 Grid topologies

The following topologies are provided:

- **Periodic blade: CC, CH, OC and OH** The considered physical domain has a cylindrical shape, parallel to the rotor axis, covering the whole rotor disk or an azimuthal sector of it. For hover simulations only an angular sector of the rotor plane containing one blade is accounted for and a perfect match between both (periodicity) planes is enforced.
- **Non-periodic blade: CC, CH, OC and OH**
- **Cap: HO** So-called cap grids deal with the tip region and tip vortex.
- **Collar: OH** A so-called collar grid topology (OH) deals with the hub region and the main blade.
- **Background:HH and OH** Cartesian background and cylindrical background grids deal with the flow about one chord length away from the blades.
- **Tip-vortex:HH and OH** Cartesian and cylindrical grids deal with the flow centred at the tip-vortex position.

3.2 Surface grid generation

Surface grid generation is the obvious basis for the volume grid generation method. The surface grid on the body is generated from the interpolation of discrete inputs of coordinates. These inputs might be obtained as output from most CAD/CAM packages or from a set of blade sections, and are organized as a network of geometrical patches linked by a connection table. The surface grid generation is performed also for the elements of such a network: a set of patch surface grids whose edges have a unique connection or are free. This network architecture allows a very flexible specification of the grid spacing in different portions of the geometrical body. A mono-block structured surface description and/or panelling of the body parts is then generated by interpolating and assembling the separate parent surface grids.

The generation of the surface grid requires the following steps:

1 Check of the patch connections to avoid non coincident vertices.
2 Manipulation of the geometrical patches to achieve a matrix-like structure of the support points.
3 Specification of the grid node number. The specification is carried out for each patch and then is modified to seek consistency according to the connection among patches.
4 Generation of the surface grid for each patch. The support points are mapped to the arc length

parameter space [13] for having adequate control of the resolution. The distribution of the grid nodes along the edges of the patches is carried out with the well-known hyperbolic tangent distributions, allowing individual control of spacing at patch edges. Two methods are embedded to generate the surface grids:

4.1 bilinear interpolation, which requires a sufficient amount of support points to be adequate.
4.2 NURB fitting which requires a much smaller number of support points to be adequate.

5 Assembling of the surface grid. In the final stage the grids generated on each patch are assembled to one surface containing the geometry as the union of the parent surface grids.

3.3 Volume grid generation

Taking into account the fact that due to the CHIMERA approach the geometric complexities are very much reduced, the development has been restricted to a relatively simple algebraic grid [2] generator. The formulation of the algebraic grid generation method is based on: the grid point at the body(slit); the normal at the body(slit); the corresponding grid point at the far field, a regularized grid point in the far field and a set of blending functions which depend on a stretching parameter. The generation takes the following steps:

1 Obtain a surface grid.
2 Generate attached slit surfaces.
3 Far field boundary generation. To account for the periodicity requirements a periodic far field boundary scaling function is applied.
4 Far field regularizations. Corners in the far field need a special treatment.
5 Near field normal definition. The near field normal is obtained by central differences which is most effective in smooth parts of the geometry. In non-smooth parts, such as at the trailing and tip edges, the normals are defined by the bisector.
6 Normal smoothing. The smoothing of the normals is performed with a Laplacian scheme.
7 Blending function scaling. The blending functions distribution along the connecting curve depend on the stretching factor which is scaled equivalent with the distance to the outer boundary.
8 For periodic grids a periodic transformation is applied to the complete grid, to map the grid to a part-cylindrical domain with matching boundary plane distributions.

For the non-boundary conforming $H\,H$ Cartesian or cylindrical grids spacing control is exercised with the hyperbolic distributions.

3.4 Volume grid quality assessment and improvements

The following local and global measures are defined for a grid: i) cross-over and negative cell volumes; ii) orthogonality (skewness); iii) smoothness and iv) aspect ratio. The quality can be improved by post application of an elliptical smoother [16]. Furthermore an a posteriori procedure [14] is developed to improve the algebraic grids (eliminate cross-over and negative cell volumes, increase orthogonality and smoothness, and obtain uniform cell volumes). The quality measures are also used in defining the priority in the CHIMERA tagging.

3.5 Volume grid dynamics

The geometric state of the grids is dynamically changing according to:

- rigid motions of the whole rotorcaft.
- rigid rotations of the whole blade assembly about the main rotor axis.
- rigid rotations of the individual blades about the hinges (flapping, pitching and lagging).
- rigid motion of the tip-vortex capture grids.
- elastic deformations of the individual blades.

The rigid motions do not require a change of the relative position of points in the same grids. For grid deformation the transfinite algebraic method [2] is applied.

3.6 Adaptation

For reasons of efficiency and accuracy the grids should be adapted to account for improved capturing of the shock waves and the vortical flow fields. Instead of developing feedback procedures (redistribution, source control terms) to create a grid more consistent with the observed physical phenomena preference is given to explicit adaptation strategies which fits naturally in the CHIMERA approach. Therefore adaptation will be applied by opting for special adaptation grids (agents). [1]

3.7 CHIMERA tagging and interpolation

The connectivity between the grids is dynamic and requires a continuous upgrading in the case of forward flight where changes might occur at each time step. The connectivity consist of: I) a colouring(tagging) activity where grid points (cells) are tagged according to:

- Inactive points (Holes): points that should not be updated in the solution phase.
- Active points: normal points.
- Flexible points (Fringes): points that get their data from support points using interpolation.

[1] In progress

and; II) the interpolation activity which is required for the fringes. The developed tagging algorithm is similar to the CMPGRD algorithm [4]. The original algorithm is improved by introducing advanced concepts: i) **quality tagging** using the quality measures to identify fringes having support boxes with the highest quality and; ii) **incremental tagging** which updates the connectivity obtained at previous time steps and reduces strongly the work in identifying the holes.

Fast hole identification procedures are developed for static applications and the initialization (preconditioning) of the aforementioned tagging procedure. They employ an analytical method whenever possible, a bounding box and a stencil walk concept. A closed k^{th} surface of a child grid is identified as the surface cutting the hole in a parent grid. The search algorithm is based on the dot product between the vector from the surface closest point P^c and the surface normal $\boldsymbol{n}_{P^c}$ at this point [9]. To speed up the basic search algorithm a bounding box concept is applied, which eliminates all points outside the box. A further decrease in CPU-time is obtained by introducing the **K-walk** strategy which is explained in figure 2. The loop over the parent cell-centres Q^p is made along the k-direction starting from the bottom and top boundary cell-centres: $Q^p{}_1$ and $Q^p{}_{NK}$. The first two points detected as holes identify the hole-segment of a k-line for a convex boundary. Table 1 presents the efficiency of the available methodologies for a typical parent-child configuration of which characteristic grid planes are depicted in figure 3.

Parent grid: $H-H$ $60 \times 60 \times 60$ cells Child grid: $O-H$ $75 \times 55 \times 20$ cells		
Procedure	**Nr. of hole-cells**	**Normalized CPU-time**
Standard	5148	1
Bounding box	5144	0.05
B. box + K-walk	5144	0.035

Table 1. Comparison of efficiency of hole identification procedures

Trilinear interpolation is applied within a hexahedral support box. This requires a reverse mapping of the support box utilizing a Newton procedure for identifying the local coordinates of the fringe point in a hexahedron. Work is in progress to improve upon this situation by the application of so-called volume spline methods [8].

4 Applications

At present the system is nearly complete and first results were already shown in [7]. Figs. 4-12 demonstrate a realistic scenery composed of OH-grids about a 4-bladed rotor which is rotating inside a background grid and performing large amplitude pitching and bending motions:

Fig. 4 shows a view from the top on the blade assembly including the background grid.

Fig. 5 shows a view from the top on the blade assembly.

Fig. 6 shows characteristic gridplanes connected to the blade.

Fig. 7 shows the bounding surface at the hub.

Fig. 8 shows characteristic gridplanes connected to the tip.

Figs. 9-11 show the deforming surface normal to the blade at the tip at several azimuthal angles. The outer boundary was fixed during the simulation.

Fig. 12 shows a close-up.

This type of grid is typical for the applications to be made using the EROS code.

5 Conclusion

The status of the common European grid generator code for the modelling of complex multi-bladed rotors has been presented. It is an essential part of the development of a complete rotorcraft simulation method: The Brite/EuRam EROS project.

Relevant results of the grid generator exploiting a CHIMERA domain decomposition on structured grids have been presented.

6 Acknowledgements

The authors would also like to thank P. Renzoni (CIRA), L. Gasparini (PMI) , S.P. Fiddes (University of Bristol) and A. Kokkalis (GKN-WESTLAND) for their contributions to the development.

7 References

1. J. Ahmad and E.P.N. Duque, 'Helicopter rotor blade computation in unsteady flows using moving overset grids', *AIAA Journal of Aircraft*, **33**(1), 54–60, (January-February 1996).
2. C.B. Allen, 'Grid Adaptation for Unsteady Flow Computations', Vol 211, Part G. I.Mech.E. Journal of Aero. Eng., (1997).
3. J.A. Benek, P.G. Buning, and J.L. Steger, 'A 3-D CHIMERA grid embedding technique', AIAA-85-1523, (1985).
4. G. Chesshire and W.D. Hensaw, 'Composite overlapping meshes for the solution of partial differential equations', *Journal of Computational Physics*, **90**, 1–64, (1990).
5. E.P.N. Duque and G.R. Srinivasan, 'Numerical simulation of a hovering rotor using embedded grids', in *Proceedings of the 48th Annual American Helicopter Society Forum*, Washington, D.C., (June 1992).
6. R. Haimes, 'VISUAL3 Users & Programmers Manual', Report, MIT, (1998).
7. M.H.L. Hounjet, C.B. Allen, L. Gasparini, L. Vigevano, and Pagano A., 'GEROS: A European Grid Generator for Rotorcraft Simulation Methods', in *Proceedings of the 6th International Conference on Grid Generation in Computational Field Simulation*, London, UK, (July 1998).
8. M.H.L. Hounjet and J.J. Meijer, 'Evaluation of Elastomechanical and Aerodynamic Data Transfer Methods for Non-planar Configurations in Computational Aeroelastic Analysis', in *International Forum on Aeroelasticity and Structural Dynamics*, pp. 11.1–11.24, Manchester, (June 1995). CEAS.
9. W.F. LaBozzetta, T.D. Gatzke, S. Ellison, G.P. Finfrock, and M.S. Fisher, 'MACGS - Towards the complete grid generation system', AIAA-94-1923-CP, (1994).
10. R.L. Meakin, 'Moving body overset grid methods for complete aircraft tiltrotor simulations', AIAA-93-3550, (1993).
11. R.L. Meakin, 'On the spatial and temporal accuracy of overset grid methods for moving body problems', AIAA-94-1925-CP, (1994).
12. K. Pahlke and J. Raddatz, 'Flexibility enhancement of Euler codes for rotor flows by chimera techniques', in *Proceedings of the 20th European Rotorcraft Forum*, Amsterdam, (NL), (October 1994).
13. J. Samareh-Abolhassani and J.E. Stewart, 'Surface grid generation in a parameter space', *Journal of Computational Physics*, **113**, 112–121, (1994).
14. B.W. Siebert and G.S. Dulikravich, 'Grid generation using a posteriori optimization with geometrically normalized functionals', AIAA-90-3048, (1990).
15. R. Stangl and S. Wagner, 'Calculation of the steady rotor flow using an overlapping embedded grid technique', in *Proceedings of the 18th European Rotorcraft Forum*, number BU-07-71, Avignon, France, (September 1992).

16. J.F. Thompson, ‘A general three-dimensional elliptic grid generation system on a composite block-structure’, *Computer Methods in Applied Mechanics and Engineering*, **64**, 377–411, (1987).

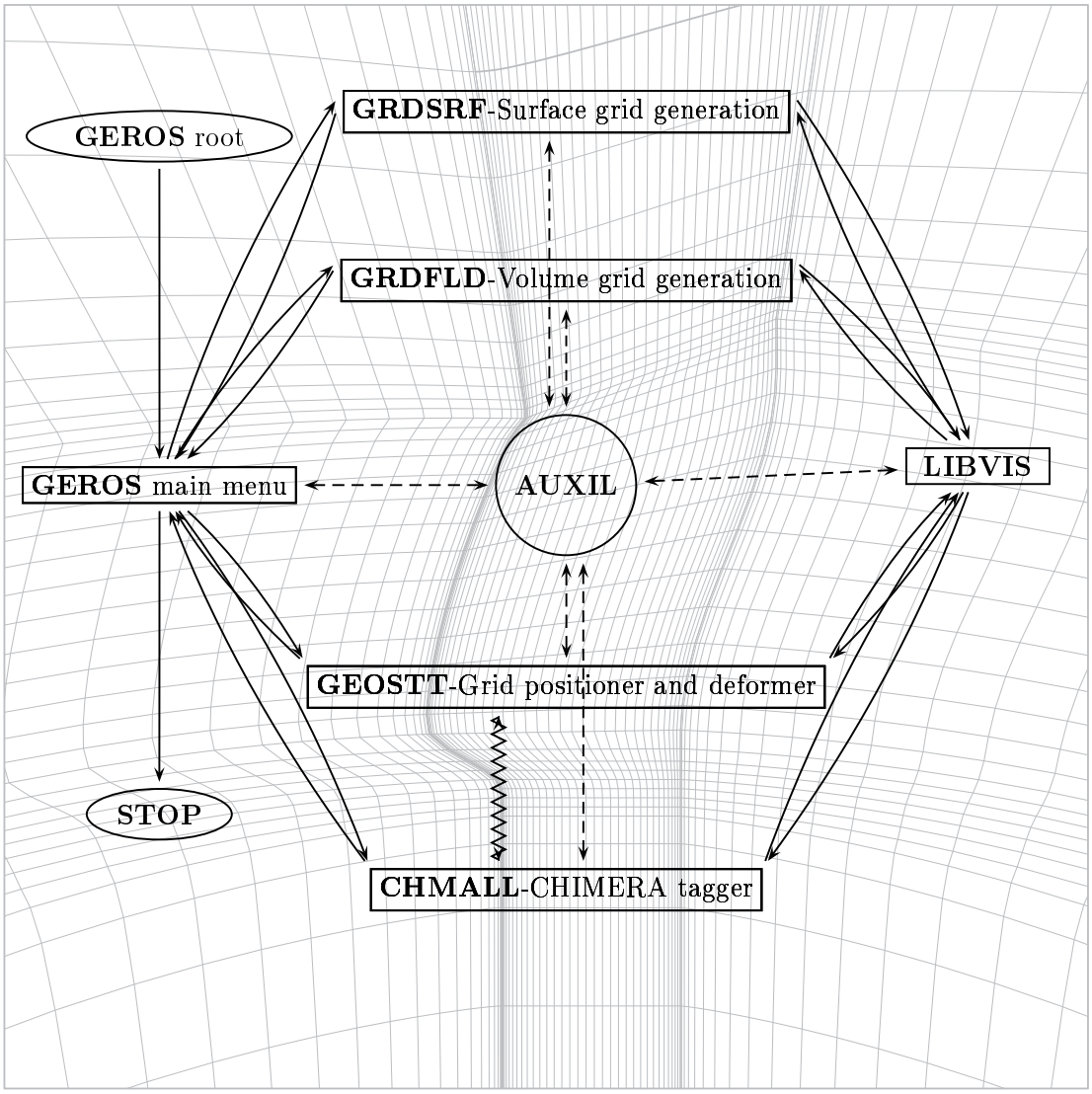

Fig. 1 GEROS structure.

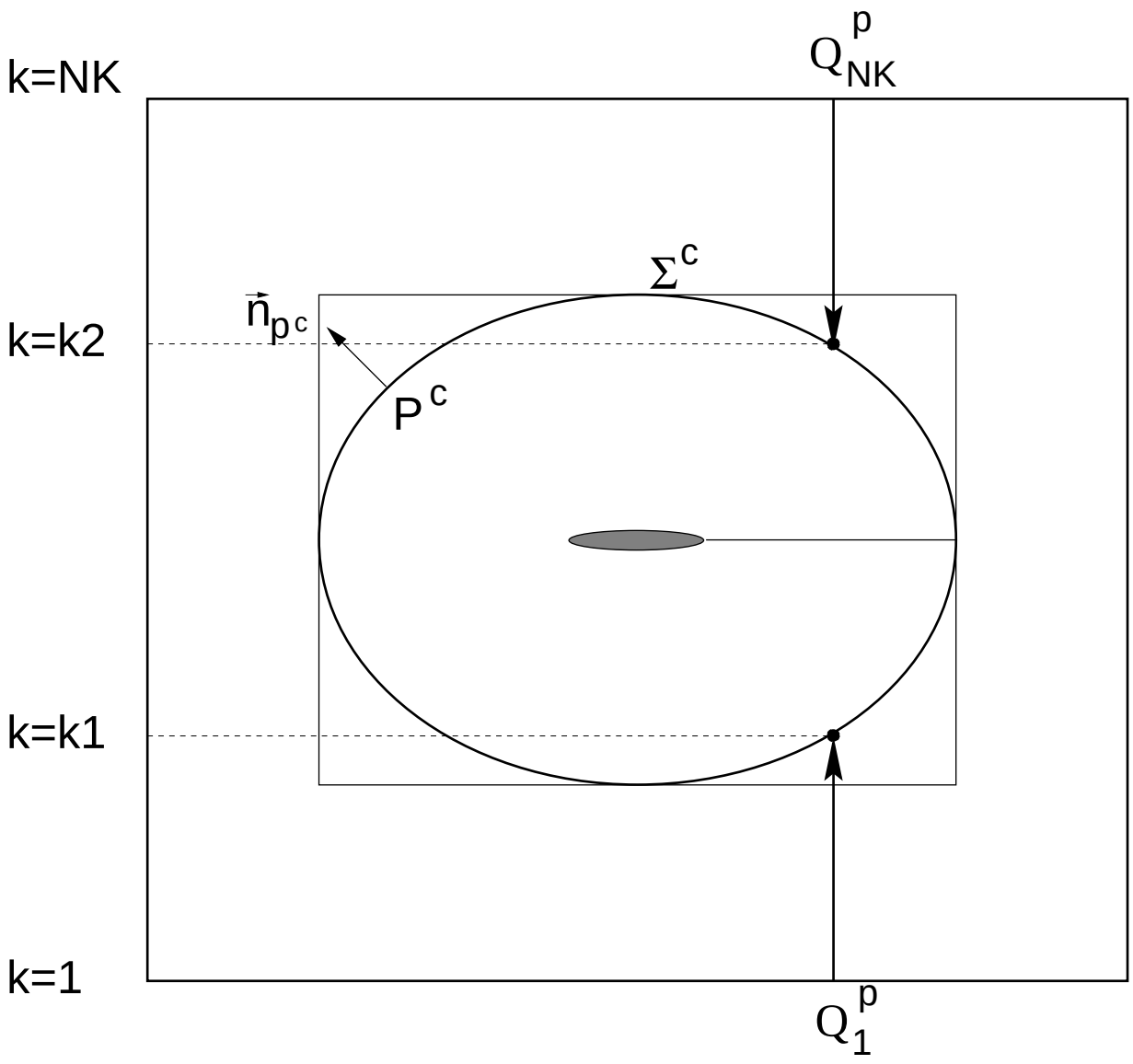

Fig. 2 Illustration for K-walk procedure

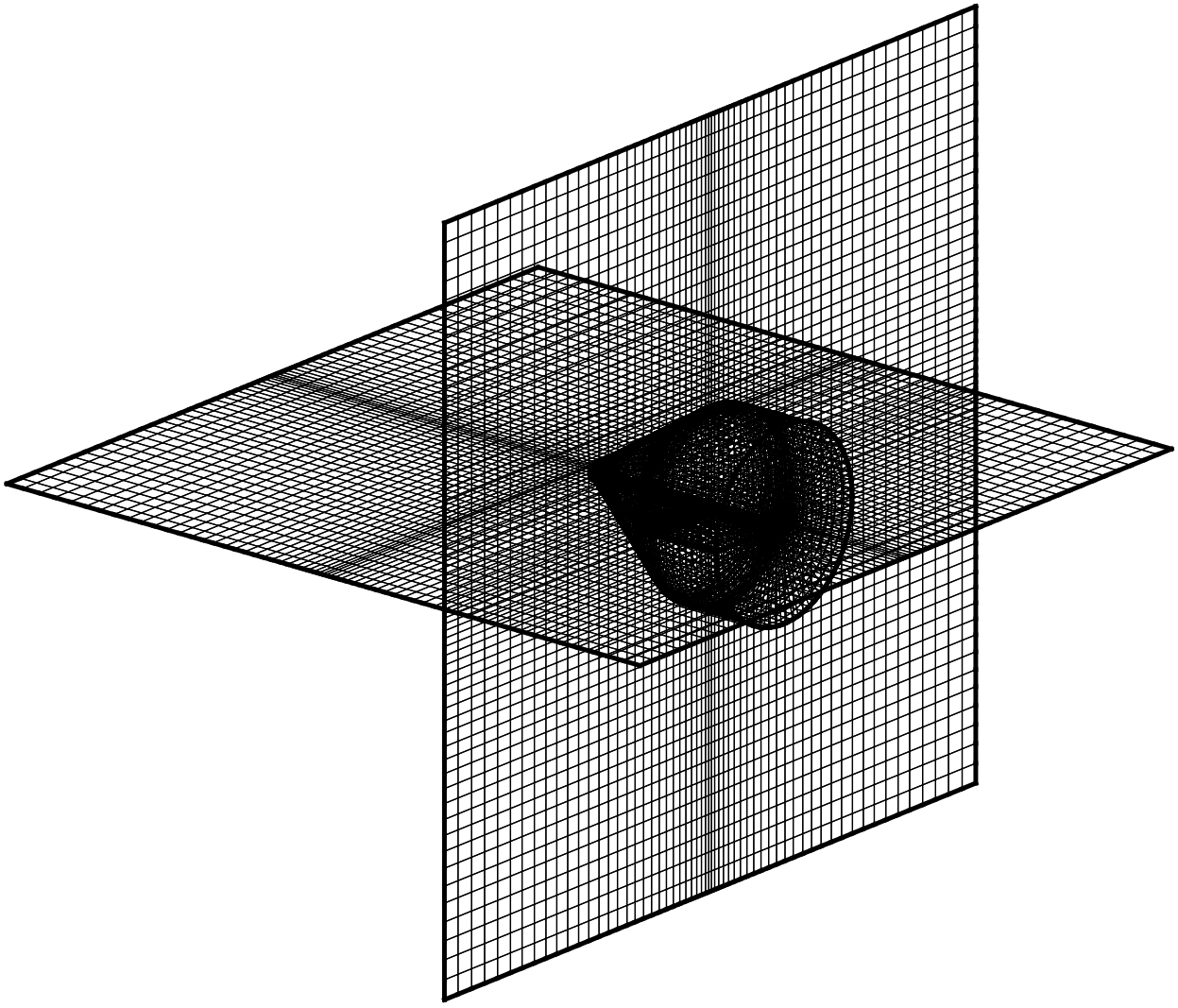

Fig. 3 Parent-child grid configuration

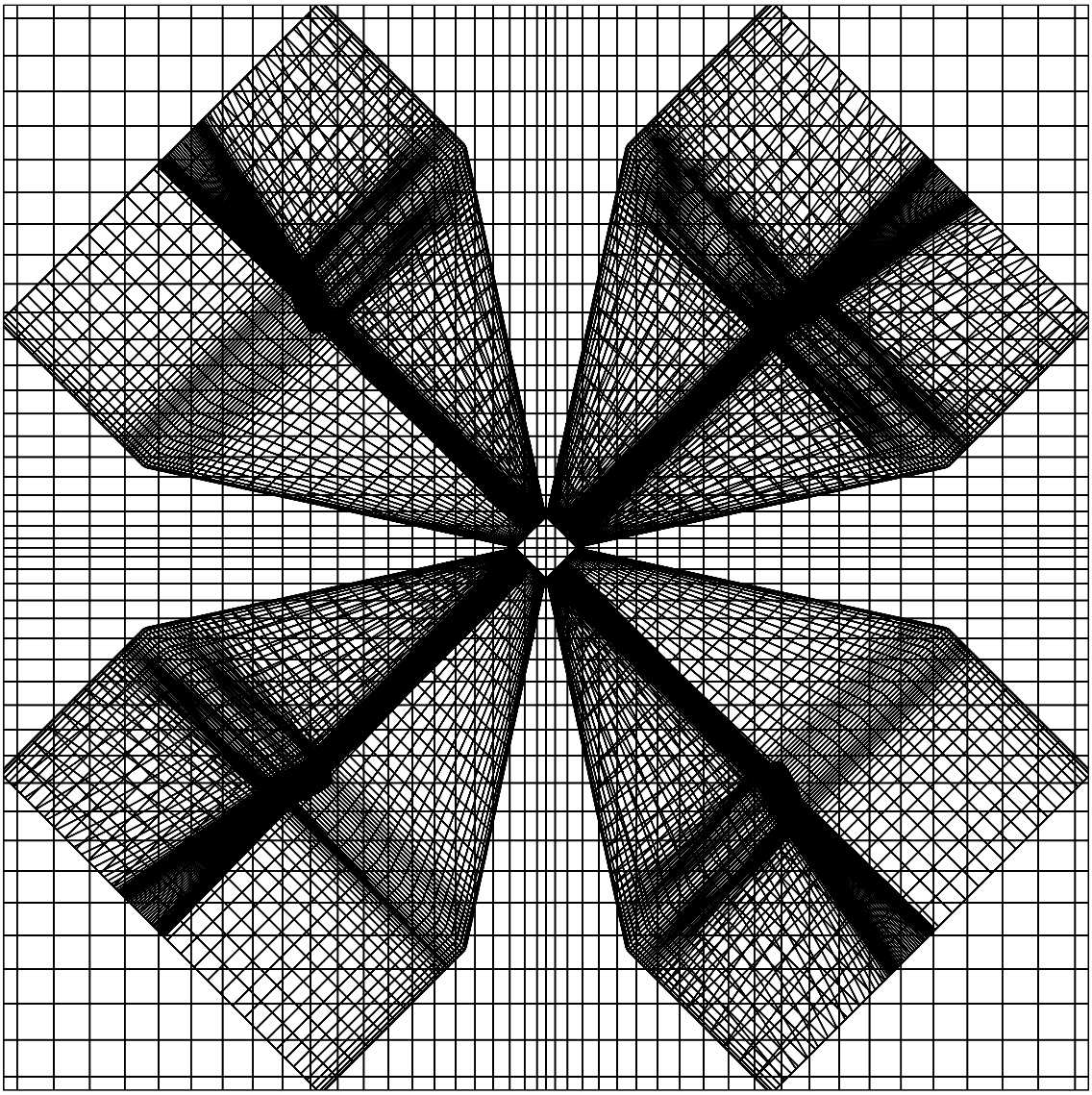

Fig. 4 Characteristic surfaces of a scenery composed of OH-grids about a 4-bladed rotor rotating inside a background grid and performing large amplitude pitching and bending motions: View from the top on the blade assembly including the background grid.

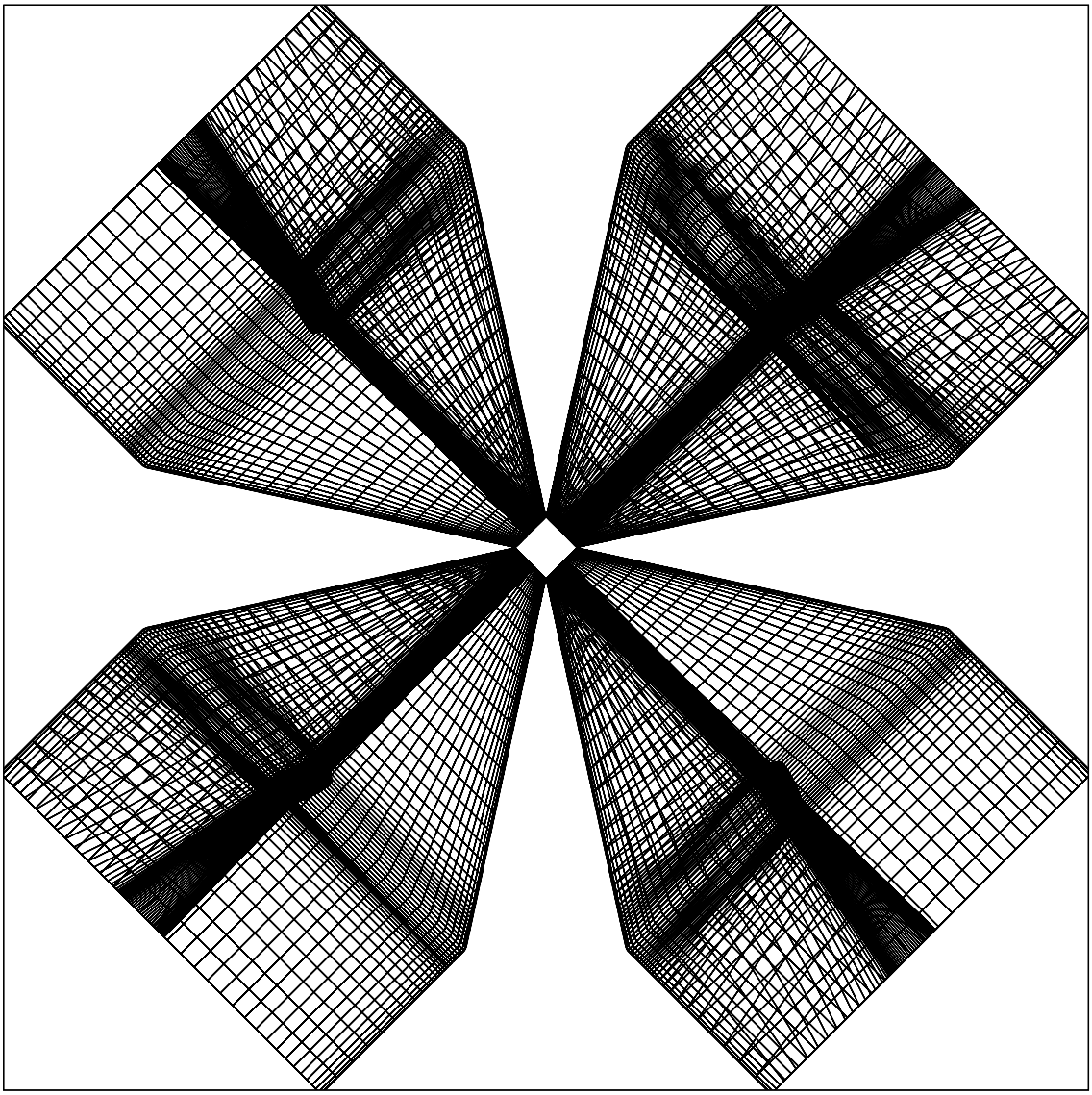

Fig. 5 Characteristic surfaces of a scenery composed of OH-grids about a 4-bladed rotor rotating inside a background grid and performing large amplitude pitching and bending motions: view from the top on the blade assembly.

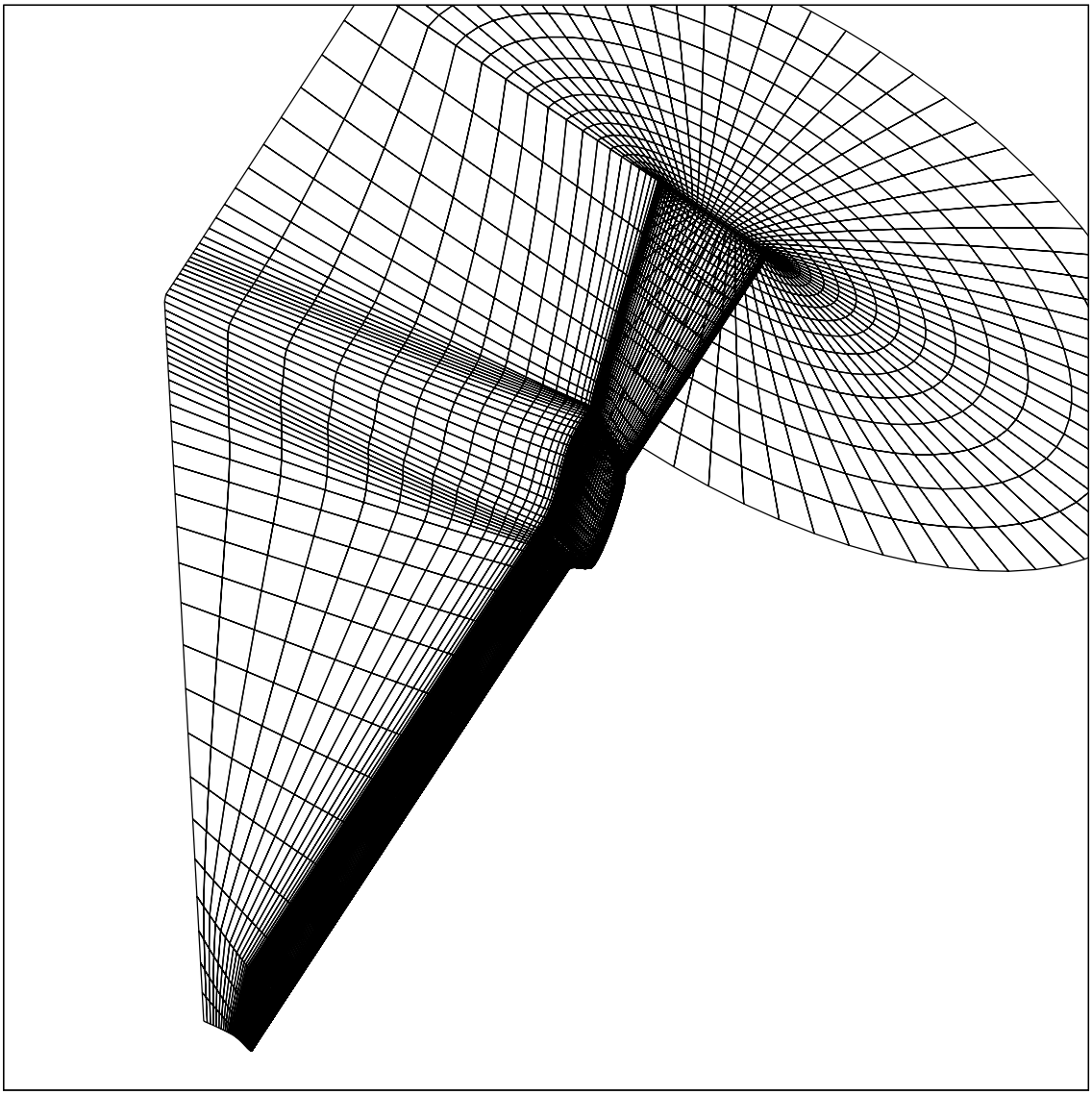

Fig. 6 Characteristic surfaces of a scenery composed of OH-grids about a 4-bladed rotor rotating inside a background grid performing large amplitude pitching and bending motions: characteristic gridplanes connected to the blade.

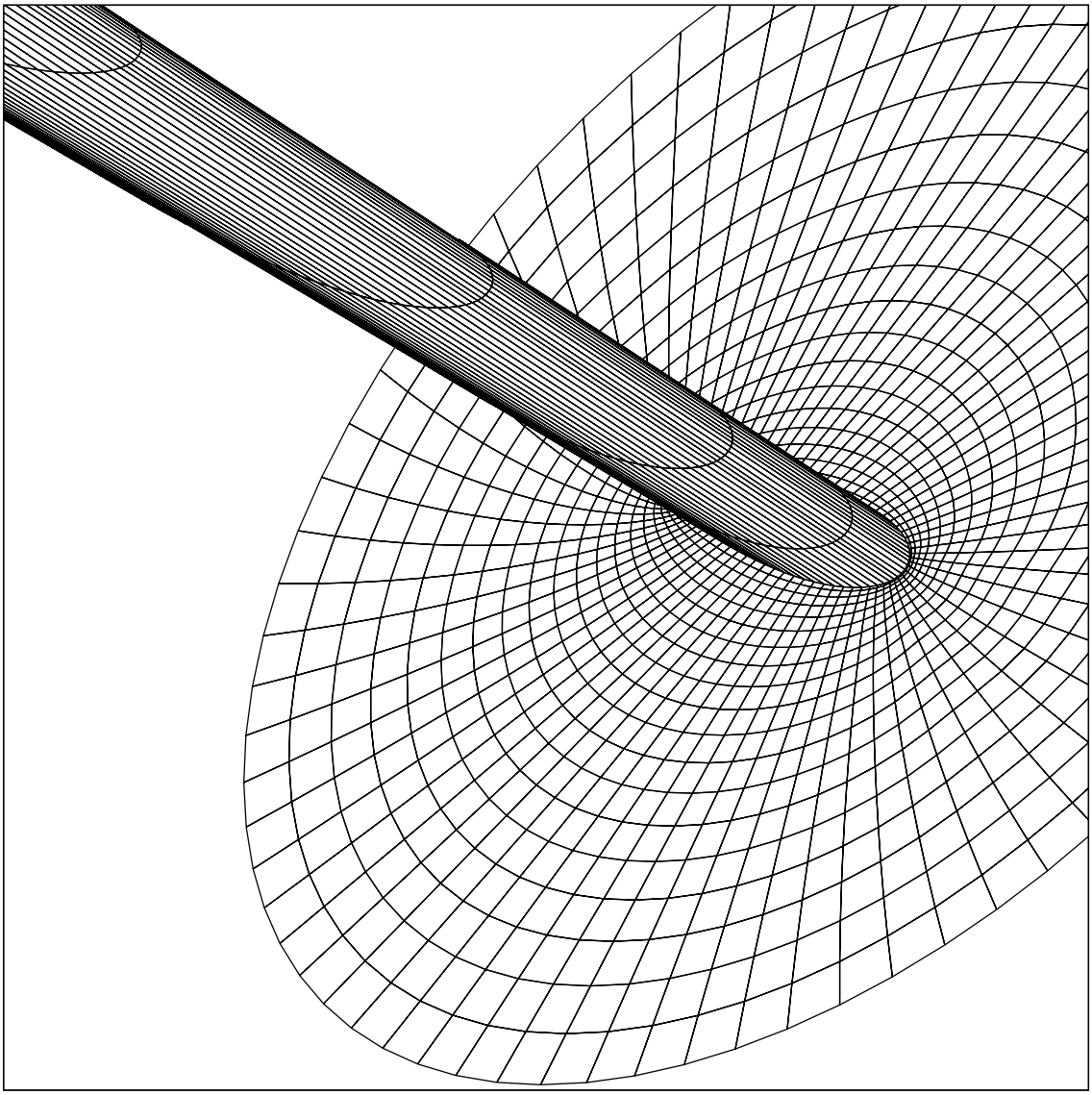

Fig. 7 Characteristic surface of a scenery composed of OH-grids about a 4-bladed rotor rotating inside a background grid and performing large amplitude pitching and bending motions: the bounding surface at the hub.

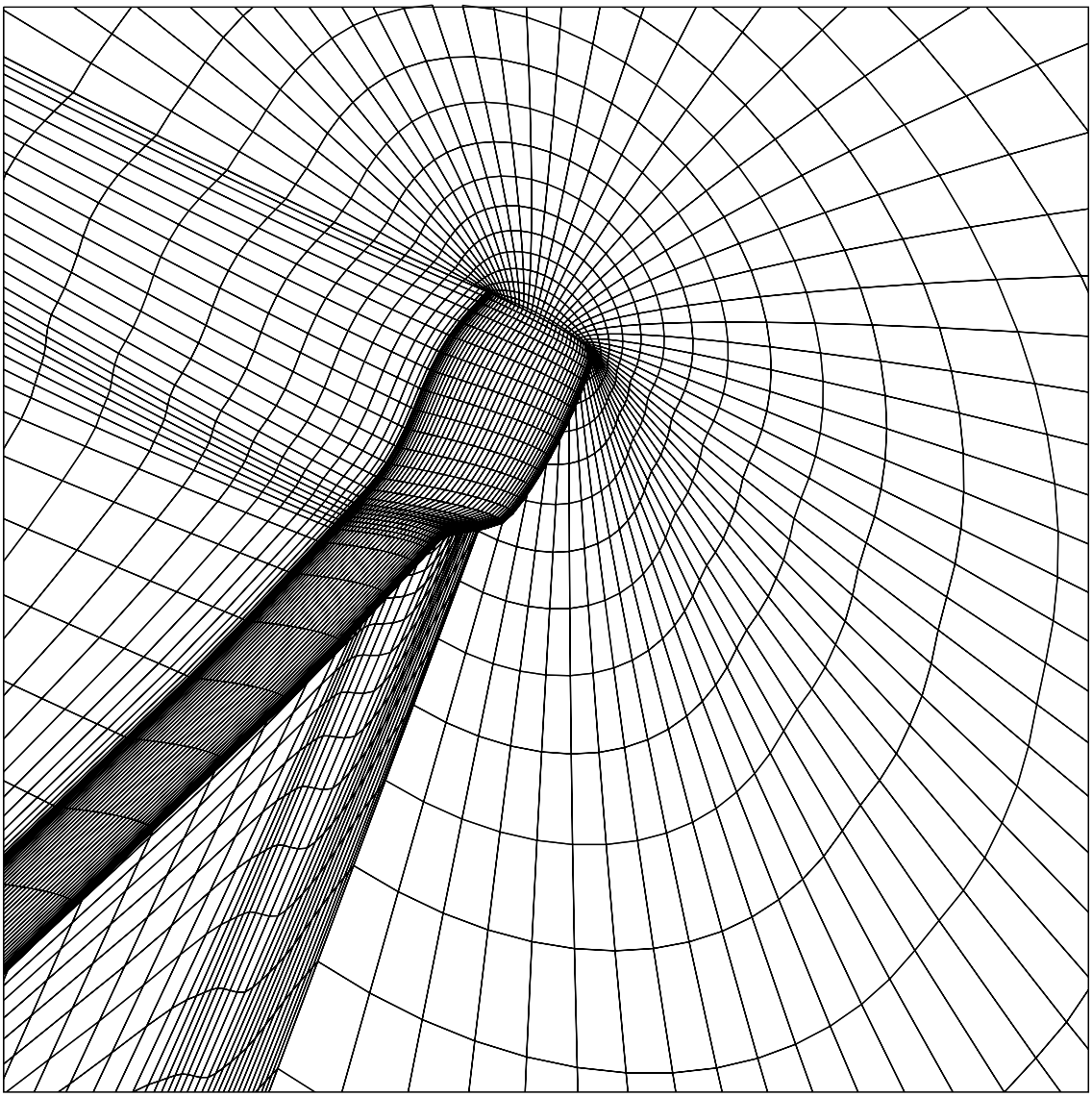

Fig. 8 Characteristic surfaces of a scenery composed of OH-grids about a 4-bladed rotor rotating inside a background grid and performing large amplitude pitching and bending motions: gridplanes connected to the tip.

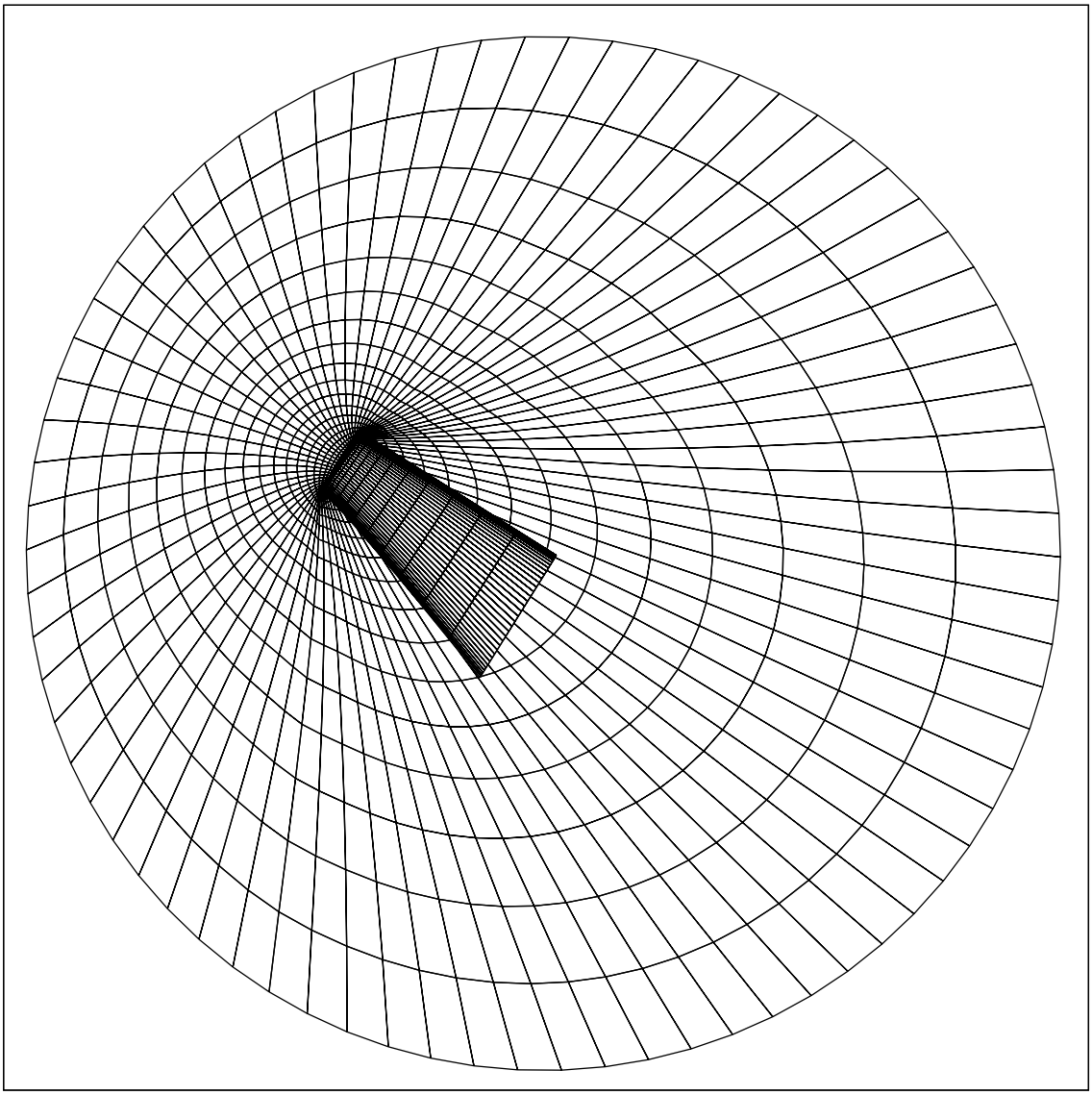

Fig. 9 Characteristic surfaces of a scenery composed of OH-grids about a 4-bladed rotor rotating inside a background grid and performing large amplitude pitching and bending motions: the deforming surface normal to the blade at the tip at an azimuthal angle of $\psi = 90$.

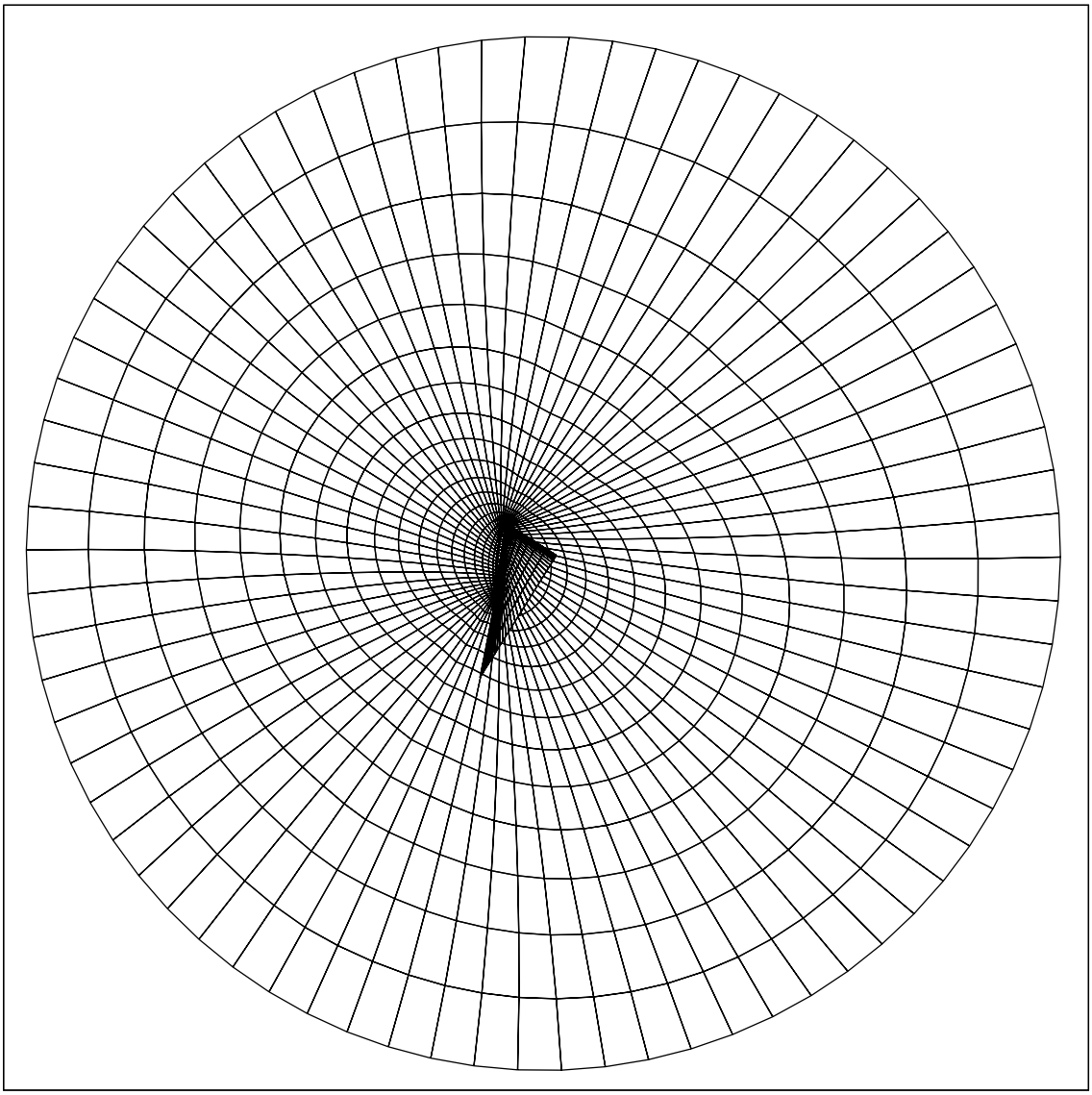

Fig. 10 Characteristic surfaces of a scenery composed of OH-grids about a 4-bladed rotor rotating inside a background grid and performing large amplitude pitching and bending motions: the deforming surface normal to the blade at the tip at an azimuthal angle of $\psi = 135$.

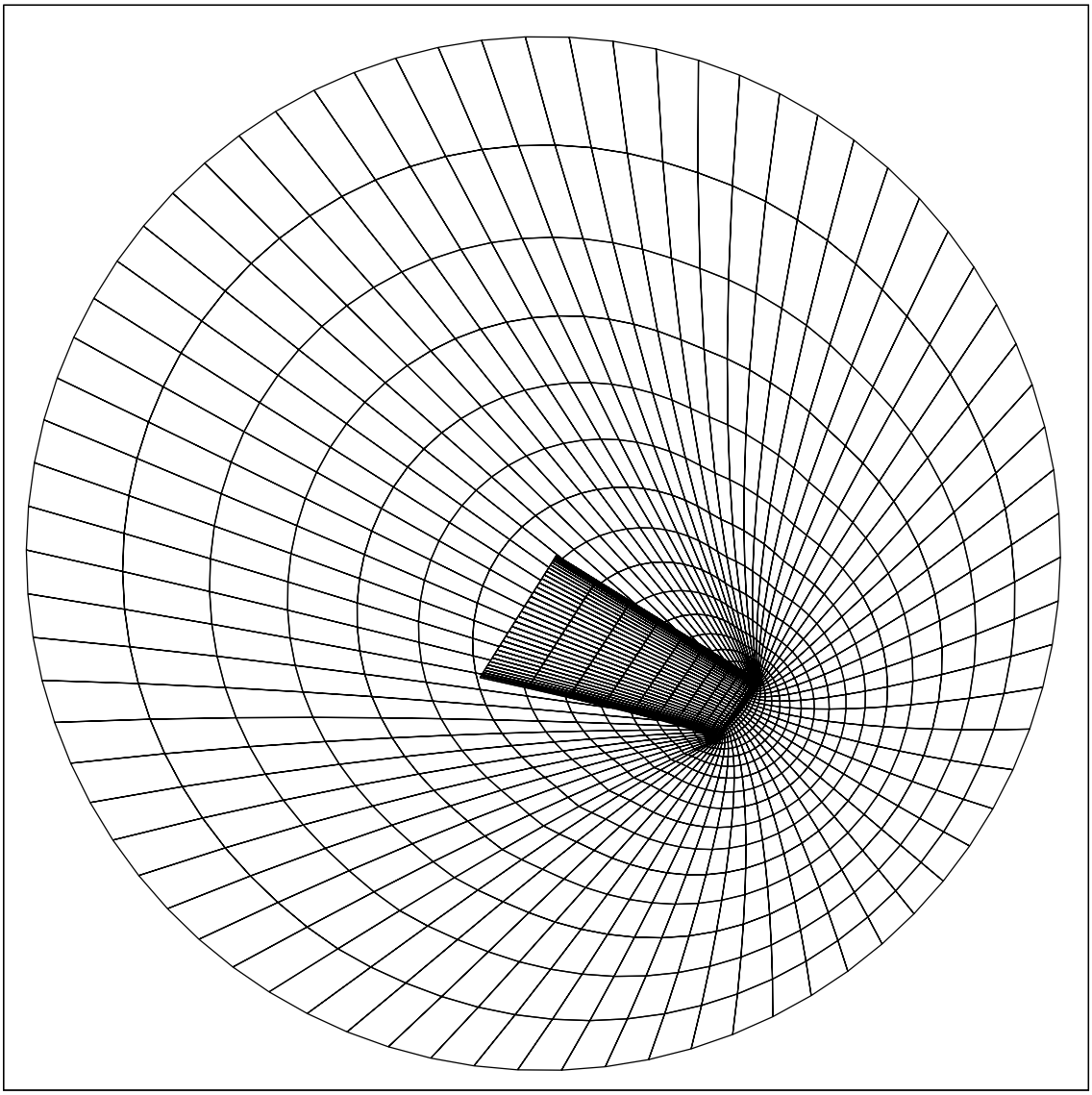

Fig. 11 Characteristic surfaces of a scenery composed of OH-grids about a 4-bladed rotor rotating inside a background grid and performing large amplitude pitching and bending motions: the deforming surface normal to the blade at the tip at an azimuthal angle of $\psi = 270$.

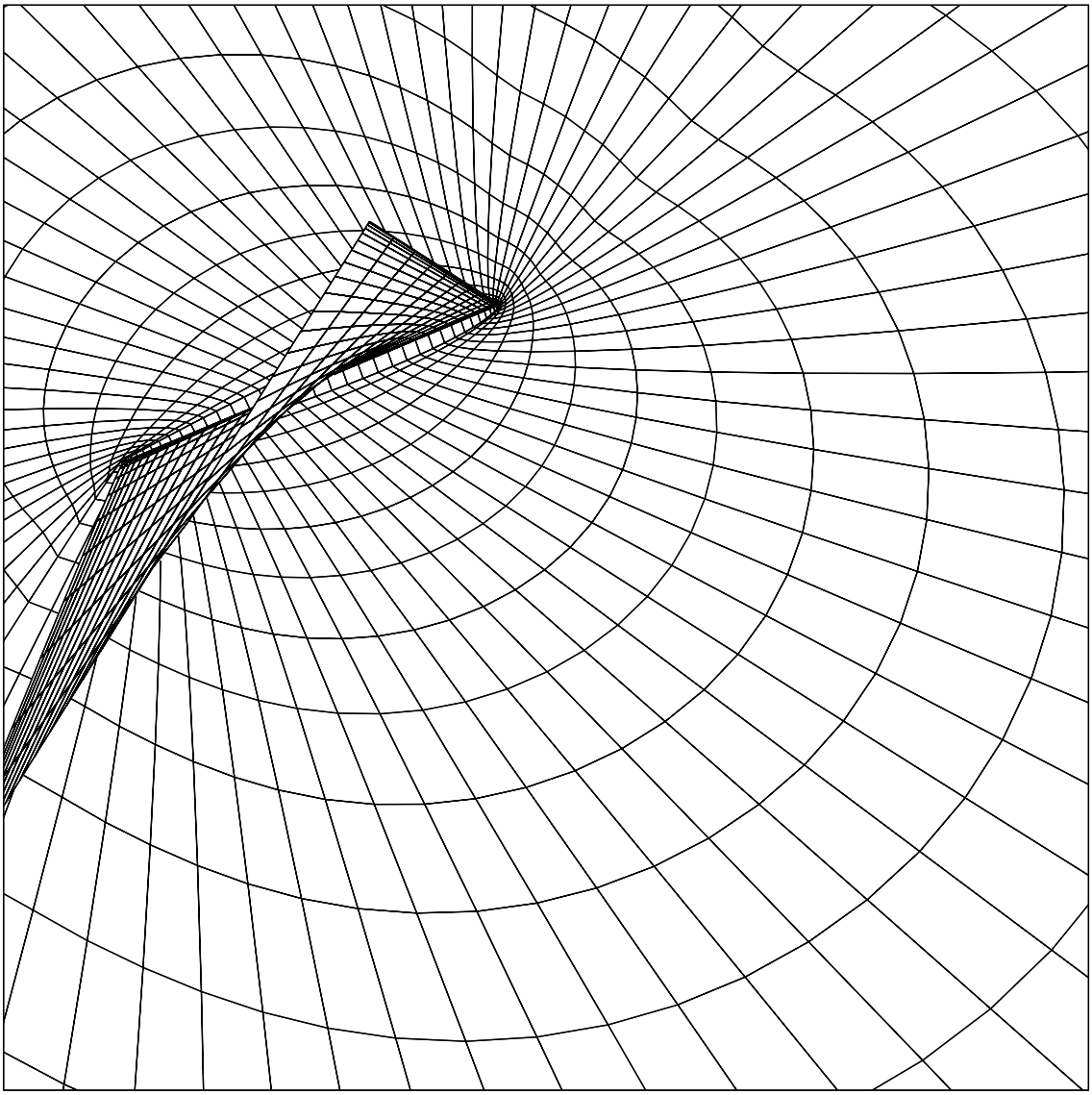

Fig. 12 Characteristic surfaces of a scenery composed of OH-grids about a 4-bladed rotor rotating inside a background grid and performing large amplitude pitching and bending motions: the deforming surface normal to the blade at the tip at an azimuthal angle of $\psi = 60.$ *(close-up)*